THE JOURNAL OF BIOLOGICAL CHEMISTRY VOL. 288, NO. 32, pp. 22985–22992, August 9, 2013

Structure and Catalytic Mechanism of Yeast 4-Amino-4-deoxychorismate Lyase*

Received for publication, April 24, 2013, and in revised form, June 29, 2013 Published, JBC Papers in Press, July 1, 2013, DOI 10.1074/jbc.M113.480335

Ya-Nan Dai, Chang-Biao Chi, Kang Zhou, Wang Cheng, Yong-Liang Jiang, Yan-Min Ren, Ke Ruan, Yuxing Chen, and Cong-Zhao Zhou[1]

From the Hefei National Laboratory for Physical Sciences at the Microscale and School of Life Sciences, University of Science and Technology of China, Hefei Anhui 230027, China

Background: *Saccharomyces cerevisiae* Abz2 is a pyridoxal 5′-phosphate-dependent lyase that converts 4-amino-4-deoxychorismate to *para*-aminobenzoate and pyruvate.
Results: Crystal structure of Abz2 reveals two basic residues, Arg-182 and Arg-255, crucial for the substrate binding and/or catalysis.
Conclusion: Abz2 leads a unique class of monomeric ADC lyases.
Significance: Provided is the first structural insight into the catalysis of a eukaryotic ADC lyase.

Saccharomyces cerevisiae **Abz2 is a pyridoxal 5′-phosphate (PLP)-dependent lyase that converts 4-amino-4-deoxychorismate (ADC) to *para*-aminobenzoate and pyruvate. To investigate the catalytic mechanism, we determined the 1.9 Å resolution crystal structure of Abz2 complexed with PLP, representing the first eukaryotic ADC lyase structure. Unlike *Escherichia coli* ADC lyase, whose dimerization is critical to the formation of the active site, the overall structure of Abz2 displays as a monomer of two domains. At the interdomain cleft, a molecule of cofactor PLP forms a Schiff base with residue Lys-251. Computational simulations defined a basic clamp to orientate the substrate ADC in a proper pose, which was validated by site-directed mutageneses combined with enzymatic activity assays. Altogether, we propose a putative catalytic mechanism of a unique class of monomeric ADC lyases led by yeast Abz2.**

Folate and coenzyme Q (ubiquinone or CoQ)[2] are very important cofactors during biological processes. Folate and its derivatives play key roles in one-carbon transfer reactions, which are involved in the biosynthesis of a wide variety of essential compounds such as methionine, purines, and thymidylate (1). Folate deficiency in humans can cause genomic instability by misincorporation of uracil into the DNA (2) and is associated with many physical disorders such as cardiovascular disease, impaired cognitive performance, and Alzheimer's disease caused by elevated homocysteine concentration (3, 4). CoQ is one of the most important electron carriers of the respiratory chain in both prokaryotes and eukaryotes (5). In addition, the reduced ubiquinol form of CoQ serves as a recyclable lipophilic antioxidant to protect membrane phospholipid layers, mitochondrial DNA, and membrane proteins against oxidative damage (6–8). Five major clinical phenotypes: encephalomyopathy, severe infantile multisystemic disease, cerebellar ataxia, isolated myopathy, and nephrotic syndrome have been reported to be associated with deficiency of coenzyme Q_{10} in humans (9). In addition, it has been demonstrated that the supplement of CoQ can protect the nigrostriatal dopaminergic system in Parkinson disease (10).

Unlike with CoQ, which is synthesized in virtually all living organisms, *de novo* biosynthesis of folate only exists in most prokaryotes, microbial eukaryotes, and plants. However, both folate and CoQ can utilize a common precursor PABA *in vivo* (11–17). In the folate synthesis pathway, PABA and 7,8-dihydro-6-hydroxymethylpterin pyrophosphate are coupled to produce 7,8-dihydropteroate, which is subsequently glutamylated to generate 7,8-dihydrofolate and ultimately reduced to yield tetrahydrofolate. The CoQ biosynthesis pathway, mostly based on the findings of Tran and Clarke (18) in yeast, usually starts with the formation of a hydroxybenzoic acid head group and a lipophilic polyisoprenoid tail (5). Alternatively, PABA could enter the CoQ biosynthesis pathway (15, 16) as a competitor of *para*-hydroxybenzoate, which has long been recognized as an aromatic precursor of the benzoquinone ring of CoQ.

The biosynthesis pathway of PABA has been identified in a few species of bacteria, microbial eukaryotes, and plants (12–14, 19–21). In most cases, PABA is synthesized from chorismate via two steps (Fig. 1): first, ADC is synthesized from chorismate and glutamine; and second, ADC is converted to PABA (22). As an exception, the PABA biosynthesis pathway in *Bacillus subtilis* contains three steps; in the first step chorismate is converted to 2-amino-2-deoxyisochorismate (23).

PABA is synthesized in *Escherichia coli* step by step via three enzymes encoded by genes designated *pabA*, *pabB*, and *pabC*, respectively (12, 22). The first step involves two reactions: PabA acts as a glutamine amidotransferase to provide the amino group to PabB, which has a synthase activity for the replacement of the hydroxyl group at the C4 position of chorismate by

* This work was supported by Ministry of Science and Technology of China Project 2012CB911000 and National Natural Science Foundation of China Grant 31170695.
The atomic coordinates and structure factors (code 4K6N) have been deposited in the Protein Data Bank (http://wwpdb.org/).
[1] To whom correspondence should be addressed. Tel. and Fax: 86-551-63600406; E-mail: zcz@ustc.edu.cn.
[2] The abbreviations used are: CoQ, coenzyme Q; PLP, pyridoxal 5′-phosphate; ADC, 4-amino-4-deoxychorismate; PABA, *para*-aminobenzoate; SeMet, selenomethionine; *Ec*PabC, *E. coli* PabC; *Lp*PabC, *L. pneumophila* PabC; *Ml*PabC, *M. loti* PabC; RMSD, root mean square deviation.

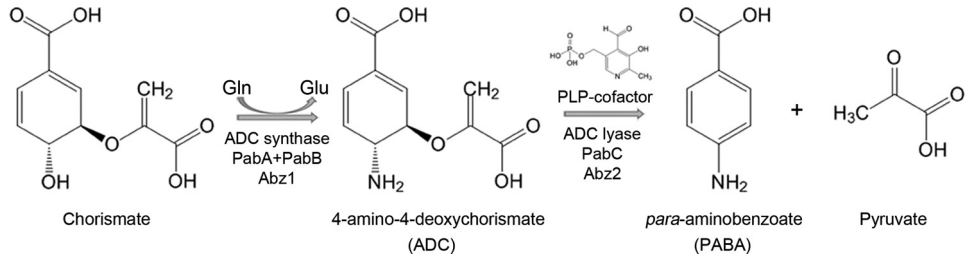

FIGURE 1. **Conversion of chorismate to *para*-aminobenzoate.** PabA, PabB, and PabC are three enzymes involved in PABA biosynthesis in *E. coli*. PabA and PabB are collectively termed ADC synthase.

the amino group. PabA and PabB normally work together to produce ADC, thus collectively termed ADC synthase. When sufficient ammonia is supplied, PabB can execute the synthase activity in the absence of PabA *in vitro* (22). In the second step, PabC serves as a PLP-dependent ADC lyase catalyzing the release of pyruvate and the aromatization of the ADC ring to give PABA. In contrast to *E. coli*, genetic and genomic data or biochemical analyses have demonstrated that ADC synthases encoded by *Streptomyces griseus* and *Plasmodium spp.* in addition to several types of fungi and plants are enzymes of two fused domains that are homologous to PabA and PabB, respectively (13, 20, 24–26). For instance, *Saccharomyces cerevisiae ABZ1/YNR033W* encodes a bifunctional ADC synthase of two domains (26), whereas *ABZ2/YMR289w* encodes an ADC lyase (*EC 4.1.3.38*) (17).

To date, four crystal structures of prokaryotic ADC lyases have been deposited in the Protein Data Bank, including *E. coli* PabC (*Ec*PabC, Protein Data Bank code 1ET0) (27), *Pseudomonas aeruginosa* PabC (Protein Data Bank code 2Y4R) (28), *Thermus thermophiles* PabC (Protein Data Bank code 2ZGI) (29), and *L. pneumophila* PabC (*Lp*PabC, Protein Data Bank code 3LUL). All of these display a similar dimeric overall fold, but with differences in the active pockets. In addition, a protein of unknown function from *Mesorhizobium loti* (Protein Data Bank code 3QQM) has been annotated as a putative amino acid aminotransferase. However, comparisons of both the overall structure and active sites indicated that it is most likely an ADC lyase.

Nevertheless, the structure of eukaryotic ADC lyase has not been determined. Here, we present the crystal structure of yeast Abz2 complexed with PLP at 1.9 Å resolution. Abz2 is composed of 374 residues, sharing no significant sequence homology with previous PabC enzymes of known structure. Structure-based computational simulation in combination with site-directed mutagenesis and enzymatic activity assays enabled us to propose a catalytic mechanism of the Abz2 enzyme. Further structural analyses enabled us to group the current ADC lyases of known structure into two classes, with Abz2 leading a unique group of monomeric ADC lyases.

EXPERIMENTAL PROCEDURES

Overexpression and Purification of Abz2 and Mutants—The *ABZ2* gene was amplified from purified genomic DNA extracted from *S. cerevisiae* S288C. The coding sequence was cloned into a pET28a-derived expression vector with an N-terminal His_6 tag and overexpressed in *E. coli* BL21 (DE3) strain (Novagen) at 37 °C using LB culture medium (10 g of NaCl, 10 g of Bacto Tryptone, and 5 g of yeast extract per liter) containing 30 μg/ml kanamycin. When the Abz2-expressing cells were grown to an $A_{600\,nm}$ of 0.8, expression of the recombinant proteins was induced with 0.2 mM isopropyl β-D-1-thiogalactopyranoside, and cell growth was continued for another 20 h at 16 °C before harvesting. The cells were collected and resuspended in the lysis buffer (100 mM NaCl, 20 mM Tris-Cl, pH 8.0). After 30 min of sonication and centrifugation at 12,000 × *g* for 30 min, the supernatant containing the soluble target protein was collected and loaded onto a nickel-chelating column (GE Healthcare) equilibrated with the binding buffer (100 mM NaCl, 20 mM Tris-Cl, pH 8.0). The target protein was eluted with 300 mM imidazole and further loaded onto a HiLoad 16/60 Superdex^{TM} 200 column (GE Healthcare) pre-equilibrated with 100 mM NaCl, 20 mM Tris-Cl, pH 8.0. Fractions containing the target protein were pooled and concentrated to 10 mg/ml for crystallization. Protein samples for enzymatic activity assays were collected at a lower concentration (1 mg/ml). Protein purity was assessed by sodium dodecyl sulfate polyacrylamide gel electrophoresis, and the protein sample was stored at −80 °C.

Selenomethionine (SeMet)-labeled Abz2 protein was expressed in *E. coli* strain B834 (DE3) (Novagen). A culture of transformed cells was inoculated into LB medium and incubated at 37 °C overnight. The cells were harvested when the $A_{600\,nm}$ reached 0.2 and were then washed twice in the M9 medium. The cells were then cultured in SeMet medium (M9 medium with 25 mg/liter L-SeMet and the other essential amino acids at 50 mg/liter) to $A_{600\,nm}$ of 0.6–0.8. The remaining steps of protein expression, purification, and storage were the same as those for the native protein.

Site-directed mutagenesis was performed by using the QuikChange site-directed mutagenesis kit (Stratagene, La Jolla, CA) with the plasmid encoding the wild-type Abz2 as the template. The mutant proteins were expressed, purified, and stored in the same manner as the wild-type protein.

Crystallization, Data Collection, and Processing—Both native and SeMet-substituted crystals of native Abz2 were grown at 16 °C using the hanging drop vapor diffusion technique, with the initial condition of mixing 1 μl of 10 mg/ml protein sample with an equal volume of the reservoir solution (20% (w/v) polyethylene glycol monomethyl ether 5,000, 0.1 M Bis-Tris, pH 6.2). Typically, crystals appeared in 1–2 days and reached the maximum size in 1 week. The SeMet derivative crystals were grown under the same conditions. The crystals were transferred to cryoprotectant (reservoir solution supplemented with

TABLE 1
Crystal parameters, data collection, and structure refinement
The values in parentheses refer to statistics in the highest bin.

	Abz2-PLP	Se-Abz2
Data collection		
Space group	$C222_1$	$C2$
Unit cell		
a, b, c (Å)	90.97, 113.89, 86.00	90.69, 114.04, 85.78
α, β, γ (°)	90.00, 90.00, 90.00	90.00, 90.66, 90.00
Resolution range (Å)	50.00–1.90 (1.97–1.90)	50.00–2.20 (2.28–2.20)
Unique reflections	35,258 (3,487)	43,953 (4,338)
Completeness (%)	99.9 (100.0)	99.3 (98.7)
$<I/\sigma(I)>$	20.0 (4.4)	22.1 (5.3)
R_{merge} (%)[a]	7.9 (42.2)	9.9 (43.0)
Average redundancy	6.2 (6.2)	6.9 (6.8)
Structure refinement		
Resolution range (Å)	36.79–1.90	
R_{factor}/R_{free} (%)[b,c]	17.4/20.2	
Number of protein atoms	2815	
Number of water atoms	260	
RMSD bond lengths (Å)[d]	0.010	
RMSD bond angles (°)	1.259	
Mean B factors (Å^2)	31.7	
Ramachandran plot (residues, %)[e]		
Most favored (%)	96.6	
Additional allowed (%)	3.4	
Outliers (%)	0	
Protein Data Bank entry	4K6N	

[a] $R_{merge} = \sum_{hkl}\sum_i|I_i(hkl) - <I(hkl)>|/\sum_{hkl}\sum_i I_i(hkl)$, where $I_i(hkl)$ is the intensity of an observation, and $<I(hkl)>$ is the mean value for its unique reflection. Summations are over all reflections.
[b] $R_{factor} = \sum_h|F_o(h) - F_c(h)|/\sum_h F_o(h)$, where F_o and F_c are the observed and calculated structure factor amplitudes, respectively.
[c] R_{free} was calculated with 5% of the data excluded from the refinement.
[d] Root mean square deviation from ideal values.
[e] Categories were defined by MolProbity.

25% glycerol) and flash-frozen with liquid nitrogen. Both the native and SeMet derivative data for single crystals were collected at 100 K in a liquid nitrogen stream using Beamline 17U with a Q315r CCD (Marresearch, Norderstedt, Germany) at the Shanghai Synchrotron Radiation Facility. All diffraction data were indexed, integrated, and scaled with HKL2000 (30).

Structure Determination and Refinement—The crystal structure of Abz2 was determined using the single-wavelength anomalous dispersion phasing method from a single SeMet-substituted protein crystal to a maximum resolution of 2.2 Å. The AUTOSOL program from PHENIX (31) was used to locate the heavy atoms, and the phase was calculated and further improved with the program SOLVE/RESOLVE (32). Electron density maps showed clear features of secondary structural elements. Automatic model building was carried out using AutoBuild in PHENIX. Afterward, the initial model was used for the molecular replacement process against the native data set at 1.90 Å with MOLREP (33). Refinement was carried out using the maximum likelihood method implemented in REFMAC5 (34) as part of CCP4i (35) program suite and rebuild interactively using the program COOT (36). The final model was evaluated with the programs MolProbity (37) and PROCHECK (38). Crystallographic parameters and data collection statistics are listed in Table 1. All figures of the structure were prepared with PyMOL (39).

High Performance Liquid Chromatography Analysis—ADC lyase activity was determined using a coupled assay by reverse phase HPLC as previously described with minor modifications (17, 22). In this assay, recombinant *E. coli* PabB was applied to generate ADC, which is the substrate of Abz2. The assays were performed in a 50-μl system containing the buffer of 50 mM Tris-Cl buffer, pH 8.5, 100 mM $(NH_4)_2SO_4$, 5 mM $MgCl_2$, and 1 mM chorismic acid (Sigma). The reactions were initiated by the addition of 10 μM PabB, and the mixture was incubated at 25 °C for 30 min followed by the removal of the protein by centrifuging with a 10-kDa cut-off filter. 20 nM wild-type Abz2 and mutants were added for further incubation at 30 °C for 30 s. Meanwhile, reaction control lacking wild-type Abz2 or mutants was also performed. Then the reactions were terminated by mixing with 10 μl of 75% acetic acid each and then were centrifuged at 12,000 $\times$ *g* for 10 min. All supernatants were then subjected in volumes of 10 μl to RP-HPLC. Buffer A (0.5% acetic acid) and Buffer B (5% acetonitrile in 0.5% acetic acid) served as the mobile phase. Buffer A was used to equilibrate the C18 column (Zorbax, 300SB_C18, 4.6 $\times$ 250 mm; Agilent). The gradient was formed as follows: 100% Buffer A for 7 min followed by 100% Buffer B for 13 min and then 100% Buffer A for 30 min for re-equilibrating the column, at a flow rate of 1 ml/min. Also, ADC, chorismic acid, and PABA standards were quantified by HPLC analysis using a series concentrations ranging from 0.5 to 2 mM and 0.125 to 1 mM, respectively.

RESULTS AND DISCUSSION

Overall Structure—Each asymmetric unit of the crystal contains one molecule of Abz2 (Fig. 2*A*). The largest total interface area between any two molecules in the crystal is 517 Å^2, which is too small to form a stable dimer. In fact, Abz2 also exists as a monomer in solution with an approximate mass of 44 kDa as determined by gel filtration chromatography. We applied the full-length Abz2 for crystallization; however, the segment of residues Met-1–Asn-22 could not be traced in the electron density map. Electrophoresis assay of the crystals confirmed that the protein had not been degraded during the crystallization process, indicating the high flexibility of this segment. The overall structure of Abz2 (Pro-23–Tyr-374) is composed of an N-terminal domain (Domain I, Pro-23–Ser-229) and a C-terminal domain (Domain II, Thr-230–Tyr-374) (Fig. 2*A*). Domain I comprises eight α-helices (α1–α8) and six β-strands (β1–β6) (Fig. 2*B*). An open β-sheet structure is formed by β-strands (β1, β5, and β6) that arrange in an antiparallel manner. Structural analysis demonstrated that apart from this β-sheet structure and two α-helices (α4 and α5), the remaining texture of Domain I displays as a unique fold referred to as the auxiliary subdomain, which is absent from all previous PabC structures (Fig. 2*A*). Three α-helices (α1–α3), combined with three short β-strands (β2–β4) that also arrange in an antiparallel manner, assemble the fold that link β1 to α4. Domain II consists of three α-helices (α9–α11) and eight β-strands (β7–β14). Three pairs of β-hairpins (β8/β9, β10/β11, and β13/β14) combined with strands β7 and β12 are sandwiched by two solvent-exposed α-helices (α10 and α11) on two sides. The PLP cofactor that is covalently bound to Lys-251 fits well in the large cleft between the two domains (Fig. 2*A*).

Structural Comparison to the Prokaryotic ADC Lyases—To determine the difference between the eukaryotic and prokaryotic ADC lyases, we superimposed Abz2 against the five crystal

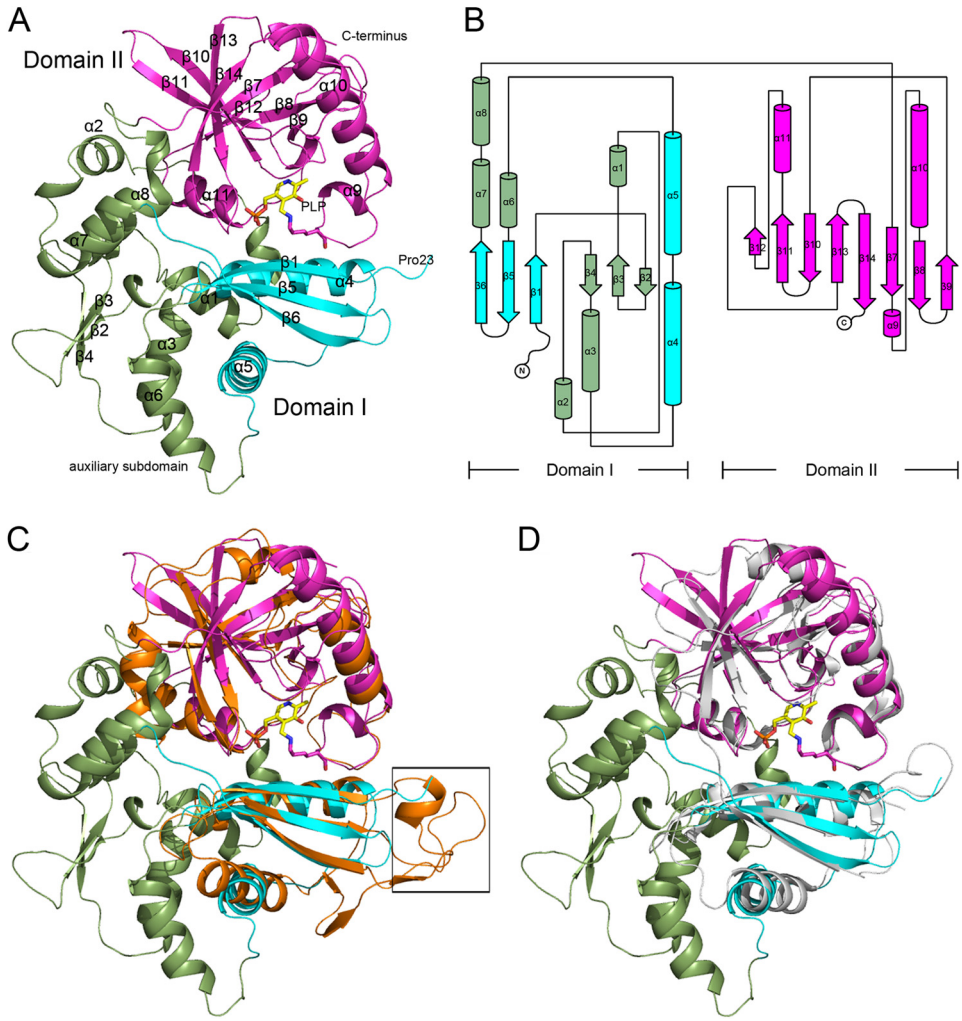

FIGURE 2. **Overall structure of yeast Abz2.** *A*, Abz2 consists of two domains. The auxiliary subdomain of Domain I is colored *green*, and the rest of it is in *cyan*. Domain II is colored *magenta*. PLP covalently bound to Lys-251 is shown as *sticks*. *B*, topology diagram of Abz2. *C*, comparison of the overall structure between Abz2 and *E. coli* PabC (*Ec*PabC, orange). The dimer interface missing from monomeric Abz2 and *Ml*PabC is *boxed*. *D*, comparison of the overall structure between Abz2 and *M. loti* PabC (*Ml*PabC, *gray*).

structures of PabC deposited in Protein Data Bank. Superposition of Abz2 against all PabC structures yielded an overall root mean square deviation (RMSD) in the range of 1.7–2.3 Å over ~190 Cα atoms, implying that they share a quite similar core structure, although they adopt very low primary sequence identities. At a closer viewpoint on Domain II, we found that Abz2 and all PabC proteins adopt a quite similar pattern of twisted antiparallel β-sheet sandwiched by two α-helices. With regard to Domain I, despite the moiety defining the active cleft, it was well superimposed to the counterparts of PabC proteins, and the auxiliary subdomain makes Abz2 unique (Fig. 2, *C* and *D*). Further structural analysis of the auxiliary subdomain demonstrated that this fold is unnecessary for the formation of active sites, and no results were obtained when a DALI search was performed. However, it is probably required to maintain the integrity and stability of Abz2. In addition, a part of the dimeric interface of *Ec*PabC is missing from Abz2 and *M. loti* PabC (*Ml*PabC) (Fig. 2, *C* and *D*).

The PLP Binding Site—A molecule of PLP cofactor is deeply buried in the cleft between Domains I and II (Fig. 3). PLP adopts the *re*-face specificity facing the protein side and is covalently linked to the catalytic residue Lys-251 by forming an internal aldimine bond (Schiff base linkage), as previously observed in other prokaryotic PabC enzymes, which are classified into PLP-dependent fold type IV enzymes (27–29).

In addition to this covalent bond, PLP is further fixed by a network of hydrogen bonds and hydrophobic interactions. The phosphate group of PLP is stabilized by eight hydrogen bonds and acts as an anchor to fix the cofactor in the active site. The hydrogen bonds are partly donated by a cluster of main chain amide groups from Gly-328, Thr-329, Met-330, Asn-360, and Gly-361. Four well ordered water molecules (Wat-1–Wat-4) located in the active site also participate in the hydrogen bond network. Wat-1 is involved in fixing an oxygen atom of the phosphate group by positioning itself to the side chain of Asn-302. Wat-2 and Wat-3 mediate the hydrogen bonds that link two other oxygen atoms of the phosphate group to the side chain amino group of Arg-128 and the side chain hydroxyl group of Thr-30. The nitrogen atom of the Schiff base linkage accepts a hydrogen bond donated from Wat-4, which in turn accepts hydrogen bonds from the main chain carboxyl group of Ile-300 and Thr-301.

In addition, the pyridine ring of PLP is sandwiched between the main chain atoms of a tripeptide segment of Ser-299, Ile-300, and Thr-301 from the side of the *si*-face, and Leu-326 from the side of the *re*-face. Glu-297 forms an ion pair with N1, the protonated nitrogen atom of the pyridine ring of PLP, and is considered to strengthen the electron withdrawing effect of the pyridine ring of PLP as an electron sink (40, 41). PLP-O3′ is fixed by a hydrogen bond with NH1 of the side chain of Arg-255.

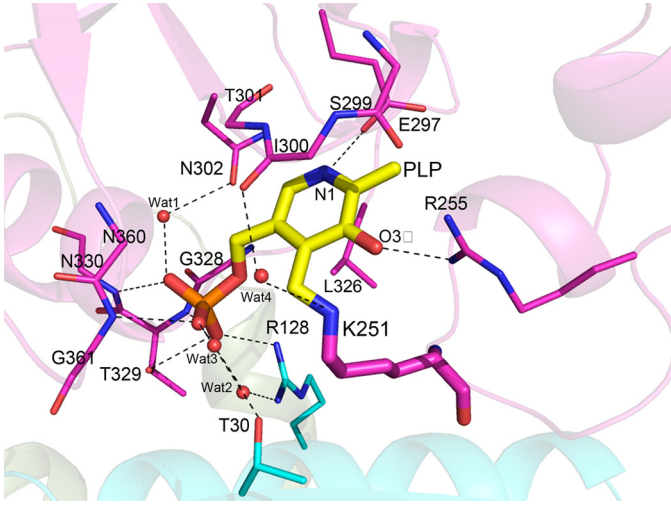

FIGURE 3. **The PLP-binding site.** PLP (*yellow*) covalently bound to catalytic residue Lys-251 (*magenta*) is shown as *bold sticks*. The PLP-binding residues are shown as *sticks*. The polar interactions are indicated by *dashed lines*.

Remodeling of the Substrate Binding Site—To elucidate the catalytic mechanism, we attempted to determine the structure of Abz2 in complex with either the substrate or product. Because the substrate ADC is not commercially available, we tried crystallizing Abz2 in complex with the product molecules (PABA and/or pyruvate) by either cocrystallization or the soaking method but failed. Alternatively, we simulated a model of a complex of apo-form Abz2 and the external aldimine, which was formed by PLP and substrate ADC using the program HADDOCK. In the modeling process, we fixed the residues Arg-255, Thr-301, Glu-297, Arg-128, Thr-329, Met-330, and Gly-361 involved in PLP binding to ensure that the external aldimine intermediate lay in a relatively reasonable pocket. Among the three output clusters, a cluster of lowest energy with four members satisfied the best interaction restraints. The overall backbone RMSD of 0.3 ± 0.2 Å for the four members indicated that the model of Abz2-ADC is somewhat reliable.

In this model, PLP fits well in the cleft between Domains I and II (Fig. 4*A*). Upon the formation of an external aldimine, the amino group of the catalytic Lys-251 is hydrogen-bonded by the phosphate group of PLP and Thr-30, which might in turn

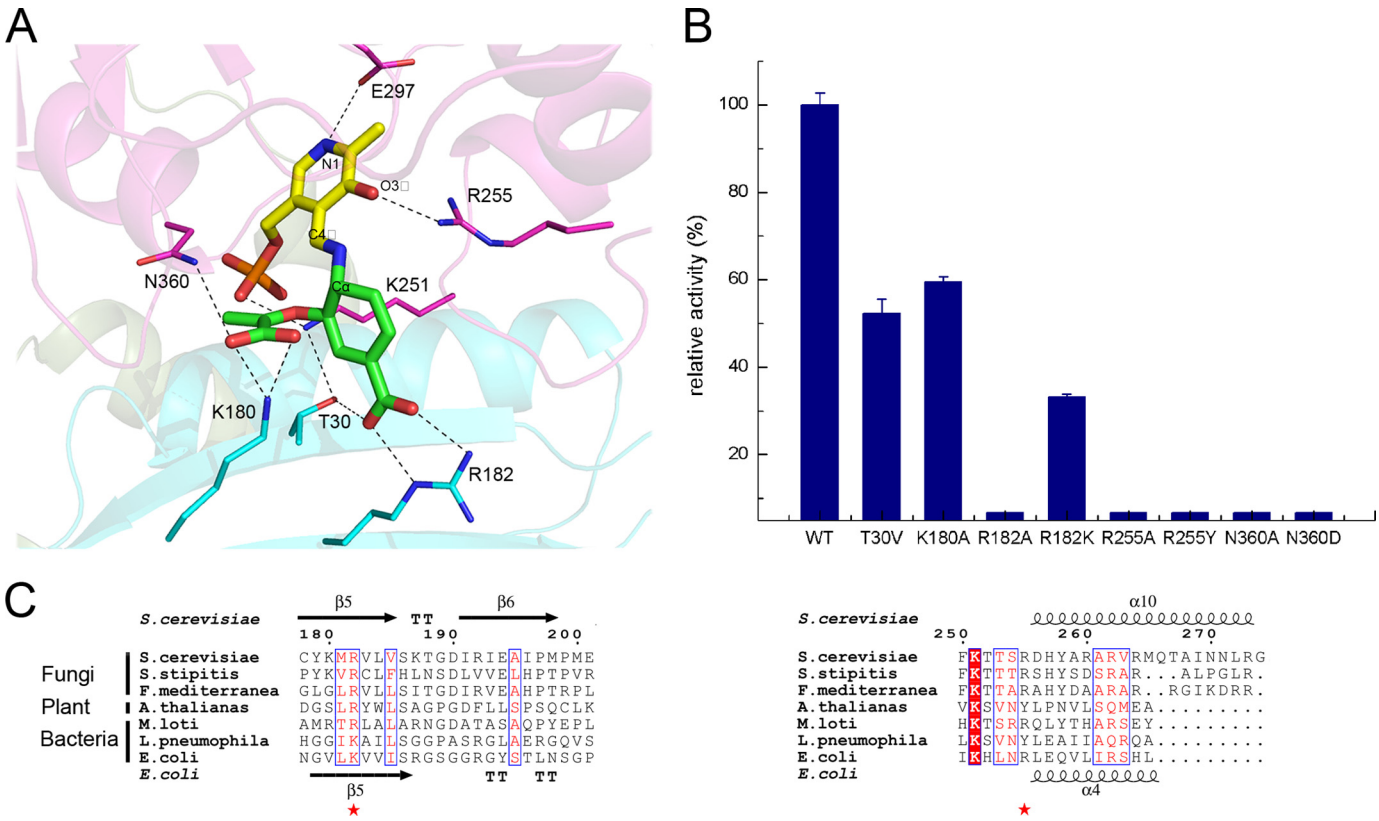

FIGURE 4. **Simulation and validation of the substrate-binding model.** *A*, a model of PLP (*yellow*)-ADC intermediate (*green*) bound to the active site of Abz2. The docked PLP-ADC intermediate and the main residues within 4 Å of PLP-ADC are shown as *sticks*. Hydrogen bonds between the active site and docked PLP-ADC are shown as *black dashes*. *B*, the relative activity of the wild-type Abz2 and mutants. *C*, multiple sequence alignment of Abz2 and homologs. The two highly conserved basic residues are indicated with *red stars*. The multisequence alignment was performed using programs ClustalW2 and ESPript. All sequences were downloaded from the NCBI database. The sequences are (NCBI accession numbers codes are in parentheses) *S. cerevisiae* Abz2 (NP_014016.1), *Scheffersomyces stipitis* CBS 6054 aminotransferase-like protein (XP_001382343.1), *Fomitiporia mediterranea* MF3/22 FOMMEDRAFT_27438 (EJD05274.1), *Arabidopsis thaliana* branched chain amino acid aminotransferase-like protein 3 (NP_200593.2), *M. loti* MAFF303099 mlr3007 (NP_104211.1), *L. pneumophila* str. Corby 4-amino-4-deoxychorismate lyase (YP_094631.1), and *E. coli* strain K-12 substrain MG1655 4-amino-4-deoxychorismate lyase (NP_415614.1).

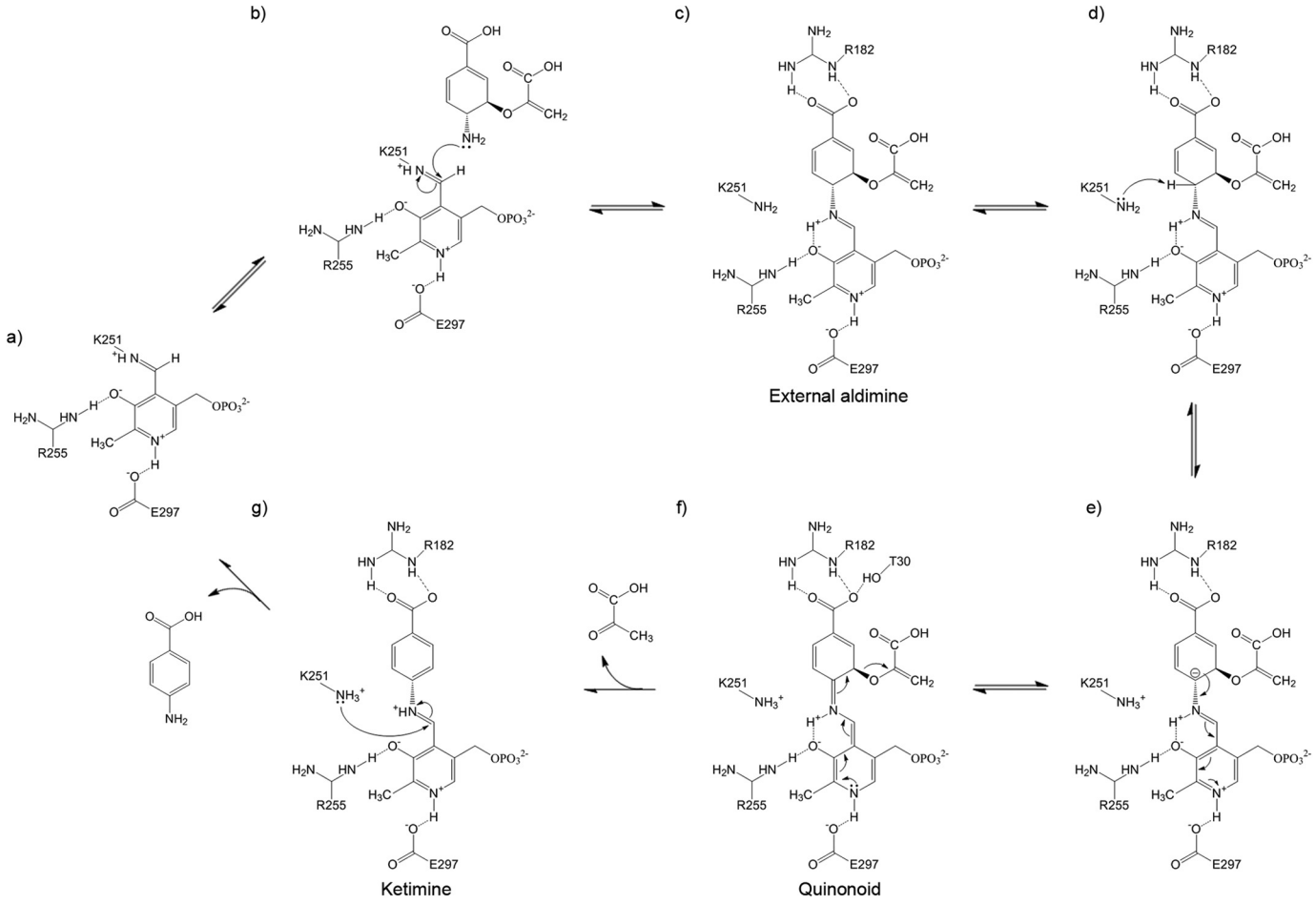

FIGURE 5. **A putative catalytic mechanism of ADC lyase.** *a*, an internal aldimine formed between Lys-251 and PLP. *b*, a nucleophilic attack of the amino group of ADC towards the C4′ of PLP. *c*, an external aldimine formed between PLP and ADC. *d*, the Cα proton of ADC abstracted by Lys-251. *e*, the Cα anion stabilized by PLP. *f*, a quinonoid intermediate. *g*, the formation of the ketimine.

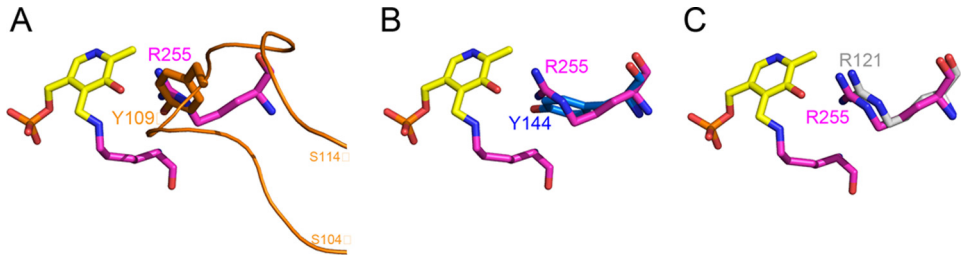

FIGURE 6. **Active site comparison of ADC lyases.** Shown is a superposition of the active site of Abz2 against that of *E. coli* PabC (*Ec*PabC, *orange*, *A*), *L. pneumophila* PabC (*Lp*PabC, *blue*, *B*), and *M. loti* PabC (*Ml*PabC, *gray*, *C*).

decrease the free energy of the external aldimine (27). Also, polar groups of ADC make extensive interactions with a cluster of hydrophilic residues (Thr-30, Lys-180, and Arg-182). Accompanying the substrate binding, the side chains of residues Lys-180 and Arg-182 are slightly shifted toward the solvent, leading to a closed functional active site (Fig. 4*A*).

To validate the docking model, we subsequently performed a series of site-directed mutageneses in combination with activity assays. Arg-182 was proposed to stabilize the substrate via two hydrogen bonds with the carboxyl group (Fig. 4*A*). Enzymatic assays showed that mutation of R182A could lead to complete inactivation of the enzyme (Fig. 4*B*), implying that it is indispensable for substrate binding and/or catalysis. Moreover, multiple-sequence alignment demonstrated that Arg-182 is quite conserved except that in some species the counterpart residue is a lysine (Fig. 4*C*). In fact the mutant R182K retained ~30% of the activity (Fig. 4*B*).

In addition, mutation of R255A also caused a complete loss of enzymatic activity (Fig. 4*B*), which might be due to the crucial role of Arg-255 in stabilizing PLP-O3′ (Fig. 3). Both the primary sequences alignment (Fig. 4*C*) and active sites comparison (discussed below, as shown in Fig. 6) indicated that a tyrosine could replace this arginine in some species. However, the enzymatic data demonstrated that the mutant of R255Y was inactive (Fig. 4*B*). Moreover, residues Thr-30, Lys-180, and Asn-360 were also hypothesized to fix the substrate via hydrogen bonding

with various groups of ADC (Fig. 4*A*). The mutants of N360A and N360D were inactive, whereas mutants T30A and K180A retained partial activity (Fig. 4*B*), indicating that these residues could also participate in catalysis to some degree. In fact, fluorescence assays demonstrated that both mutants K180A and N360A had K_d values toward pyruvic acid of ~2-fold compared with the wild-type Abz2, which further proved our docking model.

A Putative Catalytic Mechanism of Abz2—Based on the above findings, we propose a putative catalytic cycle of Abz2 (Fig. 5) following a previously hypothesized scheme (42). First, an internal aldimine is formed between the catalytic lysine (Lys-251) of Abz2 and the cofactor PLP through a Schiff base linkage (Fig. 5*a*). When approaching the substrate, the amino group of ADC triggers a nucleophilic attack toward the C4′ of PLP (Fig. 5*b*). On dissociation of PLP from Lys-251, an external aldimine is formed between PLP and ADC (Fig. 5*c*), called an imine exchange. The Cα proton of ADC is then abstracted by the noncovalently bonded Lys-251 (Fig. 5*d*), which is the only available basic active site lysine residue nearby (27). Meanwhile, PLP serves as an "electron sink" to stabilize the Cα anion by delocalizing the negative charge through a much expanded network of conjugated π-bonds and the hydrogen bond between N1 of the PLP ring and Glu-297 (Fig. 5*e*) (39, 40). Afterward, the electron density of the PLP-stabilized Cα anion intermediate improves to form a quinonoid intermediate (Fig. 5*f*), along with the release of a pyruvate and the aromatization of the six-membered ring of the substrate (Fig. 5g), also called formation of the ketimine. Finally, a molecule of PABA is released from PLP by Schiff base transfer to regenerate a starting Schiff base (Fig. 5*a*).

Structure-based Classification of ADC Lyases—As the first eukaryotic ADC lyase of known structure, Abz2 displays a monomer of two domains that form an active cleft. In contrast, the largest total interface areas in the dimeric *Ec*PabC and *Lp*PabC are 2127 and 2050 Å^2, respectively, indicating that both exist as stable dimers. PabC proteins have been classified into two groups depending upon whether the tyrosine fixing PLP-O3′ is provided from the same subunit or the neighboring subunit in the dimer (28). Taking the structure of *Ec*PabC for instance, the key residue Tyr-109′ is from a loop of the neighboring subunit (Fig. 6*A*), whereas in *Lp*PabC, the corresponding tyrosine (Tyr-144) is from the same subunit (Fig. 6*B*). As mentioned above, Arg-255 of Abz2 corresponds to Tyr-109′ of *Ec*PabC. Moreover, *Ml*PabC shares a quite similar active site composition with the monomeric Abz2, including a superimposable arginine to fix PLP-O3′ (Fig. 6*C*). In addition, *Ml*PabC is most likely a monomer that does not contain a dimeric interface corresponding to that of *Ec*PabC (Fig. 2*D*). Therefore, we could categorize the previous two groups of ADC lyase into one class, the members of which are dimers, whereas Abz2 leads another class of monomeric ADC lyases. Moreover, the two classes might be distinguished from each other by a tyrosine or an arginine to fix PLP.

REFERENCES

1. Appling, D. R. (1991) Compartmentation of folate-mediated one-carbon metabolism in eukaryotes. *FASEB J.* **5,** 2645–2651
2. Blount, B. C., Mack, M. M., Wehr, C. M., MacGregor, J. T., Hiatt, R. A., Wang, G., Wickramasinghe, S. N., Everson, R. B., and Ames, B. N. (1997) Folate deficiency causes uracil misincorporation into human DNA and chromosome breakage. Implications for cancer and neuronal damage. *Proc. Natl. Acad. Sci. U.S.A.* **94,** 3290–3295
3. Ortega, R. M., Requejo, A. M., Andrés, P., López-Sobaler, A. M., Quintas, M. E., Redondo, M. R., Navia, B., and Rivas, T. (1997) Dietary intake and cognitive function in a group of elderly people. *Am. J. Clin. Nutr.* **66,** 803–809
4. Selhub, J. (2006) The many facets of hyperhomocysteinemia. Studies from the Framingham cohorts. *J. Nutr.* **136,** 1726S–1730S
5. Olson, R. E., and Rudney, H. (1983) Biosynthesis of ubiquinone. *Vitam. Horm.* **40,** 1–43
6. Ernster, L., and Dallner, G. (1995) Biochemical, physiological and medical aspects of ubiquinone function. *Biochim. Biophys. Acta* **1271,** 195–204
7. Crane, F. L. (2001) Biochemical functions of coenzyme Q_{10}. *J. Am. Coll. Nutr.* **20,** 591–598
8. Turunen, M., Olsson, J., and Dallner, G. (2004) Metabolism and function of coenzyme Q. *Biochim. Biophys. Acta* **1660,** 171–199
9. Emmanuele, V., López, L. C., Berardo, A., Naini, A., Tadesse, S., Wen, B., D'Agostino, E., Solomon, M., DiMauro, S., Quinzii, C., and Hirano, M. (2012) Heterogeneity of coenzyme Q_{10} deficiency patient study and literature review. *Arch. Neurol.* **69,** 978–983
10. Shults, C. W., Oakes, D., Kieburtz, K., Beal, M. F., Haas, R., Plumb, S., Juncos, J. L., Nutt, J., Shoulson, I., Carter, J., Kompoliti, K., Perlmutter, J. S., Reich, S., Stern, M., Watts, R. L., Kurlan, R., Molho, E., Harrison, M., Lew, M., and Parkinson Study Group (2002) Effects of coenzyme Q_{10} in early Parkinson disease. Evidence of slowing of the functional decline. *Arch. Neurol.* **59,** 1541–1550
11. Ye, Q. Z., Liu, J., and Walsh, C. T. (1990) *p*-Aminobenzoate synthesis in *Escherichia coli*. Purification and characterization of PabB as aminodeoxychorismate synthase and enzyme X as aminodeoxychorismate lyase. *Proc. Natl. Acad. Sci. U.S.A.* **87,** 9391–9395
12. Green, J. M., and Nichols, B. P. (1991) *p*-Aminobenzoate biosynthesis in *Escherichia coli*. Purification of aminodeoxychorismate lyase and cloning of *pabC*. *J. Biol. Chem.* **266,** 12971–12975
13. Basset, G. J., Quinlivan, E. P., Ravanel, S., Rébeillé, F., Nichols, B. P., Shinozaki, K., Seki, M., Adams-Phillips, L. C., Giovannoni, J. J., Gregory, J. F., 3rd, and Hanson, A. D. (2004) Folate synthesis in plants. The *p*-aminobenzoate branch is initiated by a bifunctional PabA-PabB protein that is targeted to plastids. *Proc. Natl. Acad. Sci. U.S.A.* **101,** 1496–1501
14. Basset, G. J., Ravanel, S., Quinlivan, E. P., White, R., Giovannoni, J. J., Rébeillé, F., Nichols, B. P., Shinozaki, K., Seki, M., Gregory, J. F., 3rd, and Hanson, A. D. (2004) Folate synthesis in plants. The last step of the *p*-aminobenzoate branch is catalyzed by a plastidial aminodeoxychorismate lyase. *Plant J.* **40,** 453–461
15. Marbois, B., Xie, L. X., Choi, S., Hirano, K., Hyman, K., and Clarke, C. F. (2010) *para*-Aminobenzoic acid is a precursor in coenzyme Q_6 biosynthesis in *Saccharomyces cerevisiae*. *J. Biol. Chem.* **285,** 27827–27838
16. Pierrel, F., Hamelin, O., Douki, T., Kieffer-Jaquinod, S., Mühlenhoff, U., Ozeir, M., Lill, R., and Fontecave, M. (2010) Involvement of mitochondrial ferredoxin and *para*-aminobenzoic acid in yeast coenzyme Q biosynthesis. *Chem. Biol.* **17,** 449–459
17. Botet, J., Mateos, L., Revuelta, J. L., and Santos, M. A. (2007) A chemogenomic screening of sulfanilamide-hypersensitive *Saccharomyces cerevisiae* mutants uncovers *ABZ2*, the gene encoding a fungal aminodeoxychorismate lyase. *Eukaryot. Cell* **6,** 2102–2111
18. Tran, U. C., and Clarke, C. F. (2007) Endogenous synthesis of coenzyme Q in eukaryotes. *Mitochondrion* **7,** S62–S71
19. Chang, Z., Sun, Y., He, J., and Vining, L. C. (2001) *p*-Aminobenzoic acid and chloramphenicol biosynthesis in *Streptomyces venezuelae*. Gene sets for a key enzyme, 4-amino-4-deoxychorismate synthase. *Microbiology* **147,** 2113–2126
20. James, T. Y., Boulianne, R. P., Bottoli, A. P., Granado, J. D., Aebi, M., and Kües, U. (2002) The *pab1* gene of *Coprinus cinereus* encodes a bifunctional protein for *para*-aminobenzoic acid (PABA) synthesis. Implications for the evolution of fused PABA synthases. *J. Basic Microbiol.* **42,** 91–103
21. Zhang, Y., Bai, L., and Deng, Z. (2009) Functional characterization of the first two actinomycete 4-amino-4-deoxychorismate lyase genes. *Microbiology* **155,** 2450–2459

22. Nichols, B. P., Seibold, A. M., and Doktor, S. Z. (1989) *para*-Aminobenzoate synthesis from chorismate occurs in two steps. *J. Biol. Chem.* **264,** 8597–8601
23. Schadt, H. S., Schadt, S., Oldach, F., and Süssmuth, R. D. (2009) 2-Amino-2-deoxyisochorismate is a key intermediate in *Bacillus subtilis p*-aminobenzoic acid biosynthesis. *J. Am. Chem. Soc.* **131,** 3481–3483
24. Criado, L. M., Martín, J. F., and Gil, J. A. (1993) The *pab* gene of *Streptomyces griseus*, encoding *p*-aminobenzoic acid synthase, is located between genes possibly involved in candicidin biosynthesis. *Gene* **126,** 135–139
25. Triglia, T., and Cowman, A. F. (1999) *Plasmodium falciparum*. A homologue of *p*-aminobenzoic acid synthetase. *Exp. Parasitol.* **92,** 154–158
26. Edman, J. C., Goldstein, A. L., and Erbe, J. G. (1993) *para*-Aminobenzoate synthase gene of *Saccharomyces cerevisiae* encodes a bifunctional enzyme. *Yeast* **9,** 669–675
27. Nakai, T., Mizutani, H., Miyahara, I., Hirotsu, K., Takeda, S., Jhee, K. H., Yoshimura, T., and Esaki, N. (2000) Three-dimensional structure of 4-amino-4-deoxychorismate lyase from *Escherichia coli*. *J. Biochem.* **128,** 29–38
28. O'Rourke, P. E., Eadsforth, T. C., Fyfe, P. K., Shepherd, S. M., and Hunter, W. N. (2011) *Pseudomonas aeruginosa* 4-amino-4-deoxychorismate lyase. Spatial conservation of an active site tyrosine and classification of two types of enzyme. *PLoS One* **6,** e24158
29. Padmanabhan, B., Bessho, Y., Ebihara, A., Antonyuk, S. V., Ellis, M. J., Strange, R. W., Kuramitsu, S., Watanabe, N., Hasnain, S. S., and Yokoyama, S. (2009) Structure of putative 4-amino-4-deoxychorismate lyase from *Thermus thermophilus* HB8. *Acta Crystallogr. Sect. F Struct. Biol. Cryst. Commun.* **65,** 1234–1239
30. Otwinowski, Z., and Minor, W. (1997) Processing of x-ray diffraction data collected in oscillation mode. *Methods Enzymol.* **276,** 307–326
31. Adams, P. D., Afonine, P. V., Bunkóczi, G., Chen, V. B., Davis, I. W., Echols, N., Headd, J. J., Hung, L. W., Kapral, G. J., Grosse-Kunstleve, R. W., McCoy, A. J., Moriarty, N. W., Oeffner, R., Read, R. J., Richardson, D. C., Richardson, J. S., Terwilliger, T. C., and Zwart, P. H. (2010) PHENIX. A comprehensive Python-based system for macromolecular structure solution. *Acta Crystallogr. D Biol. Crystallogr.* **66,** 213–221
32. Terwilliger, T. C., and Berendzen, J. (1999) Automated MAD and MIR structure solution. *Acta Crystallogr. D Biol. Crystallogr.* **55,** 849–861
33. Vagin, A., and Teplyakov, A. (2010) Molecular replacement with MOLREP. *Acta Crystallogr. D Biol. Crystallogr.* **66,** 22–25
34. Murshudov, G. N., Vagin, A. A., and Dodson, E. J. (1997) Refinement of macromolecular structures by the maximum-likelihood method. *Acta Crystallogr. D Biol. Crystallogr.* **53,** 240–255
35. Collaborative Computational Project, Number 4 (1994) The CCP4 Suite. Programs for protein crystallography. *Acta Crystallogr. D Biol. Crystallogr.* **50,** 760–763
36. Emsley, P., and Cowtan, K. (2004) Coot. Model-building tools for molecular graphics. *Acta Crystallogr. D Biol. Crystallogr.* **60,** 2126–2132
37. Davis, I. W., Leaver-Fay, A., Chen, V. B., Block, J. N., Kapral, G. J., Wang, X., Murray, L. W., Arendall, W. B., 3rd, Snoeyink, J., Richardson, J. S., and Richardson, D. C. (2007) MolProbity. All-atom contacts and structure validation for proteins and nucleic acids. *Nucleic Acids Res.* **35,** W375–W383
38. Laskowski, R. A., Macarthur, M. W., Moss, D. S., and Thornton, J. M. (1993) Procheck. A program to check the stereochemical quality of protein structures. *J. Appl. Crystallogr.* **26,** 283–291
39. DeLano, W. (2002) *The PyMOL Molecular Graphics System*, De Lano Scientific, San Carlos, CA
40. Jansonius, J. N. (1998) Structure, evolution and action of vitamin B_6-dependent enzymes. *Curr. Opin. Struct. Biol.* **8,** 759–769
41. Eliot, A. C., and Kirsch, J. F. (2004) Pyridoxal phosphate enzymes. Mechanistic, structural, and evolutionary considerations. *Annu. Rev. Biochem.* **73,** 383–415
42. Green, J. M., Merkel, W. K., and Nichols, B. P. (1992) Characterization and sequence of *Escherichia coli pabC*, the gene encoding aminodeoxychorismate lyase, a pyridoxal phosphate-containing enzyme. *J. Bacteriol.* **174,** 5317–5323